Acta Biomaterialia 188 (2024) 157–168

Contents lists available at ScienceDirect

Acta Biomaterialia

journal homepage: www.elsevier.com/locate/actbio

Full length article

Thermosensitive chitosan-based hydrogel: A vehicle for overcoming the limitations of nose-to-brain cell therapy

Doddy Denise Ojeda-Hernández[a], Susana Velasco-Lozano[b,c], José M. Fraile[b], J.C. Mateos-Díaz[d], Francisco J. Rojo[e,f,g], María Soledad Benito-Martín[a], Belén Selma-Calvo[a], Sarah de la Fuente-Martín[a], Marina García-Martín[a], María Teresa Larriba-González[a], Mercedes Azucena Hernández-Sapiéns[h], Alejandro A. Canales-Aguirre[h], Jordi A. Matias-Guiu[a,i], Jorge Matias-Guiu[a,i], Ulises Gomez-Pinedo[a,*]

[a] Laboratorio de Neurobiología, Instituto de Neurociencias. Instituto de Investigación Sanitaria San Carlos (IdISSC), Hospital Clínico San Carlos, Madrid, Spain
[b] Instituto de Síntesis Química y Catálisis Homogénea (ISQCH), CSIC-Universidad de Zaragoza, C/ Pedro Cerbuna, 12, 50009 Zaragoza, Spain
[c] Aragonese Foundation for Research and Development (ARAID), Av. Ranillas, 1-D, 50018 Zaragoza, Spain
[d] Unidad de Biotecnología Industrial. Centro de Investigación y Asistencia en Tecnología y Diseño del Estado de Jalisco (CIATEJ), Zapopan, Mexico
[e] Centro de Tecnología Biomédica, Universidad Politécnica de Madrid, Pozuelo de Alarcón, 28223 Madrid, Spain
[f] Departamento de Ciencia de Materiales, ETSI Caminos, Canales y Puertos, Universidad Politécnica de Madrid, 28040 Madrid, Spain
[g] Grupo de Biomateriales y Medicina Regenerativa, Instituto de Investigación Sanitaria San Carlos (IdISSC), Hospital Clínico San Carlos, Madrid, Spain
[h] Unidad de Evaluación Preclínica, Biotecnología Médica y Farmacéutica, Centro de Investigación y Asistencia en Tecnología y Diseño del Estado de Jalisco (CIATEJ), Guadalajara, Mexico
[i] Servicio de Neurología, Instituto de Neurociencias. Instituto de Investigación Sanitaria San Carlos (IdISSC), Hospital Clínico San Carlos, Universidad Complutense de Madrid, Spain

ARTICLE INFO

Article history:
Received 7 May 2024
Revised 31 August 2024
Accepted 3 September 2024
Available online 7 September 2024

Keywords:
Functionalized chitosan$_1$
Thermosensitive hydrogel$_2$
Mucoadhesive$_3$
Nose-to-brain$_4$
Cell therapy$_5$
Bioactive vehicle$_6$

ABSTRACT

Cell therapy is a promising strategy for treating neurological pathologies but requires invasive methods to bypass the blood–brain barrier restrictions. The nose-to-brain route has been presented as a direct and less invasive alternative to access the brain. The primary limitations of this route are low retention in the olfactory epithelium and poor cell survival in the harsh conditions of the nasal cavity. Thus, using chitosan-based hydrogel as a vehicle is proposed in this work to overcome the limitations of nose-to-brain cell administration. The hydrogel's design was driven to achieve gelification in response to body temperature and a mucosa-interacting chemical structure biocompatible with cells. The hydrogel showed $a < 30$ min gelation time at 37 °C and >95 % biocompatibility with 2D and 3D cultures of mesenchymal stromal cells. Additionally, the viability, stability, and migration capacity of oligodendrocyte precursor cells (OPCs) within the hydrogel were maintained *in vitro* for up to 72 h. After the intranasal administration of the OPCs-containing hydrogel, histological analysis showed the presence of viable cells in the nasal cavity for up to 72 h post-administration in healthy athymic mice. These results demonstrate the hydrogel's capacity to increase the residence time in the nasal cavity while providing the cells with a favorable environment for their viability. This study presents for the first time the use of thermosensitive hydrogels in nose-to-brain cell therapy, opening the possibility of increasing the delivery efficiency in future approaches in translational medicine.

Statement of significance

This work highlights the potential of biomaterials, specifically hydrogels, in improving the effectiveness of cell therapy administered through the nose. The nose-to-brain route has been suggested as a non-invasive way to directly access the brain. However, delivering stem cells through this route poses a challenge since their viability must be preserved and cells can be swept away by nasal mucus. Earlier attempts

Abbreviations: CS, Chitosan; SA, Succinic acid; FA, Ferulic acid; GP, Genipin; SA-CS, Succinic acid-grafted chitosan; SA/FA-CS, Succinic and ferulic acid-grafted chitosan; SA/FA-CS-GP, Succinic and ferulic acid-grafted chitosan crosslinked with genipin; WJ, Wharton's Jelly; iPS-OPCs, Induced pluripotent stem cell-derived oligodendrocyte precursor cells; EGFP-iPS-OPCs, EGFP-expressing iPS-OPCs.

* Corresponding author.
E-mail address: u.gomez.pinedo@gmail.com (U. Gomez-Pinedo).

https://doi.org/10.1016/j.actbio.2024.09.002
1742-7061/© 2024 The Author(s). Published by Elsevier Ltd on behalf of Acta Materialia Inc. This is an open access article under the CC BY-NC-ND license (http://creativecommons.org/licenses/by-nc-nd/4.0/)

at intranasal cell therapy have shown low efficiency, but still hold promise to the future. The hydrogels designed for this study can provide stem cells with a biocompatible environment and adhesion to the nasal atrium, easing the successful migration of viable cells to the brain.

© 2024 The Author(s). Published by Elsevier Ltd on behalf of Acta Materialia Inc.
This is an open access article under the CC BY-NC-ND license
(http://creativecommons.org/licenses/by-nc-nd/4.0/)

1. Introduction

Over the last few years, the potential of cell therapy has been widely demonstrated for neurological disorders [1]. Cell therapy has been shown to provide neuroprotection through diverse mechanisms, such as immunomodulation, neuromodulation, scavenging of toxic metabolic byproducts, secretion of growth factors, and normalization of metabolic pathways [1,2]. Among the most employed cells for such disorders are mesenchymal stromal cells (MSCs), which can be obtained from different sources, such as bone marrow, dental pulp, or adipose tissue. MSCs can be easily obtained and exhibit low immunogenicity, leading to their extensive evaluation in preclinical studies and clinical trials [3]. Other types of cells can also be used for specific purposes, for example, oligodendrocyte precursor cells (OPCs) are effective in enhancing remyelination in the brain and spinal cord and promoting oligodendrogenesis [4–6]. One of the limitations of cell therapy targeting the central nervous system (CNS) is the presence of the blood-brain barrier (BBB), which restricts access to systemically administered substances, including cells. To bypass the BBB, local administration can be performed through invasive methods, such as intracerebral and intrathecal injections. Alternatively, the intranasal route has been studied and shown to facilitate cell access to the CNS [7].

Studies of intranasally administered cell therapy have shown promising preclinical results for neurological disorders [8]. However, the therapeutic effectiveness of the administered cells may be compromised by mucociliary clearance and cell viability loss due to the harsh conditions of the nasal mucosa. Therefore, it is imperative to design vehicles for nose-to-brain cell delivery that can provide cells (stem, adult, or pluripotent) with a protective environment and enhance their interaction with the nasal mucosa to increase cell retention. These vehicle formulations must promote mucopenetration, allowing cells to pass through the nasal mucus and adhere to the olfactory epithelium, thereby minimizing clearance [9].

The use of mucoadhesive polymers, such as chitosan (CS), has been proposed in drug delivery to increase the residence time at the mucosal surface and facilitate the permeation of various drugs into the CNS [10]. CS is a bioactive polymer, composed of D-glucosamine and N-acetyl-D-glucosamine, that has become one of the preferred natural polymers in many fields [11]. It possesses intrinsic properties like biocompatibility and biodegradability, along with antimicrobial, antioxidant, antitumoral, and wound healing, making CS a versatile and popular ingredient for biomedical applications [12]. Particularly, the interest in CS and its derivatives for nose-to-brain applications has increased due to its penetration enhancement ability and mucoadhesive capacity, complemented by its tunable controlled release and capability to penetrate the BBB [13]. Consequently, different CS-based delivery systems have been developed for nasal drug delivery, such as nanoparticles, hydrogels, and nanolipid-based hydrogels [14–16]. The mucoadhesive capacity of CS has been attributed to electrostatic interactions between protonated amino groups and negatively charged sialic acid moieties on mucin [17]. However, the solubility and mucoadhesive strength of CS are limited at physiological pH [18]. This limitation can be counteracted by substituting functional groups in the molecular structure of CS. Commonly, the primary amine at C-2, primary hydroxyl at C-6, and secondary hydroxyl at C-3 are used for grafting substituents to provide CS with new properties [19]. Therefore, functionalization has become a key strategy to overcome the limiting features of CS for nasal administration [18]. Both covalent and non-covalent functionalization methods are used, with covalent methods producing more stable products [20]. Although many molecules have been employed as substituents for CS functionalization, dicarboxylic acids (*e.g.* succinic acid, SA) have significantly improved the biomaterial's functional properties [21,22]. It is important to consider that functionalizing CS will not only modify its chemical and mechanical properties but also modulate its biological behavior. Functionalization of CS with molecules selected for their biological activities, such as hydroxycinnamic acids (*e.g.* ferulic acid, FA), has resulted in products with enhanced biological properties and increased applicability in the biomedical field [20].

In this study, chitosan (CS) is functionalized with succinic and ferulic acids to create a thermosensitive hydrogel designed as a vehicle for nose-to-brain cell therapy. The hydrogel is formulated by incorporating genipin to achieve rapid gelation (under 30 min) in response to body temperature, along with a mucosa-interacting chemical structure that is biocompatible with cells. The primary objective is to develop a biocompatible vehicle that provides a protective microenvironment for cells in the nasal cavity and enhances mucopenetration, applicable to various models of neurological pathologies. Biocompatibility is assessed using 2D and 3D cell cultures, and *in vivo* intranasal administration is tested in athymic mice. While this study does not include a therapeutic evaluation, it demonstrates for the first time the feasibility of using hydrogels for nose-to-brain cell therapy by proving their biocompatibility, cell-migration capacity, and cell-retention ability in the nasal atrium, as well as observing evidence of cell presence in the brain using transfected markers or immunohistochemistry.

2. Materials and methods

2.1. Materials

CS (<75 % deacetylation degree; >75 % purity) of two molecular weights: low molecular weight (LMw; 50–190 kDa) and medium molecular weight (MMw; 190–375 kDa); (E)-3-(4–hydroxy-3-methoxyphenyl)prop–2-enoic acid (FA; >98 % purity), butanedioic acid (SA; >99 % purity), N-(3-Dimethylaminopropyl)-N′-ethyl carbodiimide hydrochloride (EDC), 4-Dimethylaminopyridine (DMAP), N,N-Dimethylformamide (DMF), Dimethyl sulfoxide (DMSO), acetic acid, genipin, sodium bicarbonate, and ninhydrin were obtained from Sigma (France). Phosphate Buffer Saline (PBS) was obtained from Gibco (Spain). Wharton's Jelly (WJ) was obtained from Histocell (GAGs extract; Ref. CC036).

For MSCs culture, Dulbecco's Modified Eagle Medium (DMEM/F-12), Fetal Bovine Serum (FBS), and Anti-Anti were obtained from Gibco (Spain), and cell culture-treated T75 flasks were obtained from Corning. For induced pluripotent stem cell-derived OPCs (iPS-OPCs) culture, Human Oligodendrocyte Progenitor Cells iPC derived Culture (Non-Viral) Growth Media with Serum and Antibiotics, and Human Oligodendrocyte Progenitor Cells iPC derive Culture (Non-Viral) Extracellular Matrix T75 Flasks were obtained from

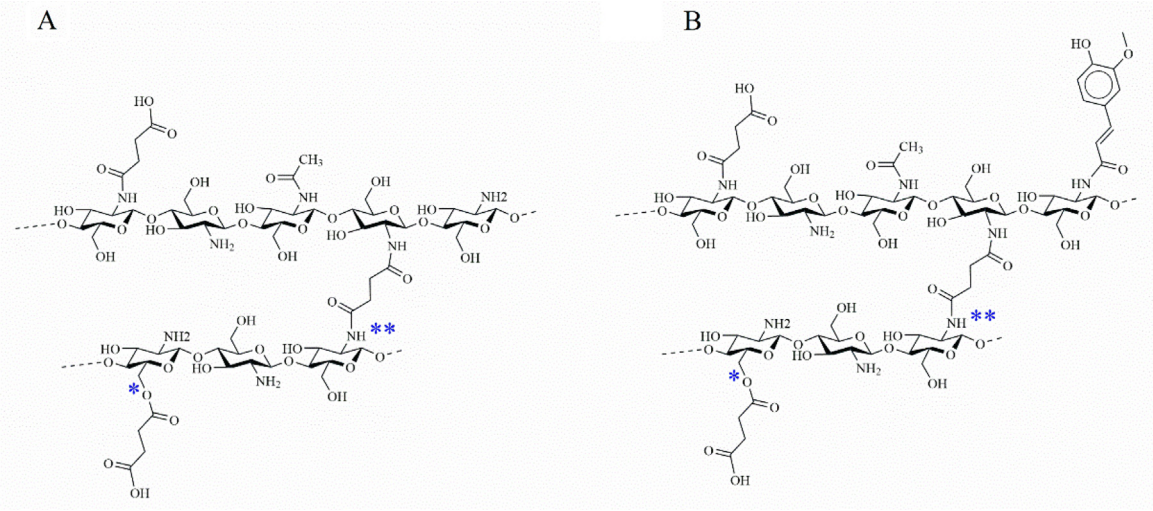

Fig. 1. Expected molecular structure from functionalized CS. Products of Step 1 (A) and Step 2 (B) reactions. *Succinic acid could bind to primary hydroxyl function due to the addition of DMAP catalyst, depending on substituent concentration. **Due to its dicarboxylic nature, succinic acid may also bind by its two ends, leading to a crosslinking between polymeric chains.

Celprogen (Netherlands). For cytotoxicity assays, MTT (ScienCell) and Live/Dead™ Cell Imaging (Invitrogen, Thermo Fisher Scientific) kits were used. ECM-gel® was obtained from Sigma-Aldrich (France).

2.2. Chitosan functionalization

CS was functionalized with SA and FA as previously reported [23]. Briefly, CS was dissolved in 1 % (v/v) acetic acid to a final concentration of 1.2 % (w/v). Functionalization occurred in two steps, with SA grafted first, followed by FA (Fig. 1).

In Step 1, SA was mixed with EDC (10 % excess relative to the substituent) and, when indicated, DMAP (5% mol) in DMF (10 % v/v of the reaction volume). This mixture was added to the CS solution and incubated for 17 h at 30 °C with constant stirring. The product, SA-grafted CS (SA-CS), was recovered by precipitation with 96 % ethanol (Fig. 1A)

In Step 2, SA-CS was dissolved in 1 % (v/v) acetic acid. FA and EDC (10 % excess relative to the substituent) were mixed in DMF (10 % v/v of the reaction volume) and added to the SA-CS solution. DMAP was not used in this step. The reaction was incubated for 3 h at 30 °C with constant stirring. The final product, SA and FA-grafted CS (SA/FA-CS), was precipitated and washed three times with 75 % ethanol (Fig. 1B).

Different ratios of the substituents to CS's free amines (0.25:1, 0.5:1, 1:1, and 2:1) were evaluated to assess the degree of functionalization under the reaction conditions used. The employed ratios for each step and the obtained amine substitution degree are summarized in Table S1.

2.2.1. Selection of the substituent's concentration in functionalized chitosan

LMw CS functionalization reaction was performed up to Step 1 to evaluate different SA:CS's free amine ratios over the functionalization degree and solubility in 1X PBS at pH 7.2. The employed SA:CS ratios were: 2:1, 1:1, and 0.5:1. Changes in solubility were studied by turbidimetry [24], where 10 mg of vacuum-dried SA-CS were incubated with 1 mL of PBS at room temperature for 30 min. Samples were mixed by pipetting and 0.2 mL were placed into a 96-well plate. Absorbance was measured at 400 nm using a spectrophotometer (FLUOstar Omega, BMG Labtech).

2.3. Formulation of the thermosensitive hydrogel

The components employed for the thermosensitive hydrogel formulation were selected according to previous reports where genipin is employed for CS crosslinking [25,26], also, considering the conditions for keeping cell viability. The composition of the formulation consisted of SA/FA-CS, PBS, sodium bicarbonate, genipin dissolved in DMSO, and water. The formulation was optimized through variations in the component's proportions, in search of solubility, a short gelation time, and biocompatibility with MSCs.

2.3.1. Gelation time

A reaction buffer consisting of 0.5X PBS plus 0.14% w/v sodium bicarbonate was prepared, where 0.5 M HCl was used to adjust pH to 7.2 or 6.5 values. Gelation time was evaluated at different concentrations of MMw SA/FA-CS (2 %, 4 %, 8 %, and 12% w/v) dissolved in pH 7.2 reaction buffer, and to varying concentrations of genipin in DMSO (0.01, 0.05, 0.1, and 0.2% w/v genipin with 1 %, 5 %, 10 %, and 20 % v/v DMSO). The sol–gel transition was determined by the inverted tube test [15], The 1.5 mL tubes containing 0.5 mL of the sample mixtures were incubated in a water bath at 37 °C. The bath temperature was controlled employing a hotplate stirrer (RT2 Advanced Hotplate Stirrer, Thermo Scientific™) with a temperature probe (PT100, SN-8-4 connector sensor, Thermo Scientific™). Every 5 min the samples were briefly taken out of the bath and checked by tilting the tubes. Gelation was recorded when no flow was observed within the tilted test tubes.

Gelation time was also determined for the selected formulation, consisting of 2% w/v of LMw SA/FA-CS in reaction buffer at pH 6.5 and 0.01 % genipin.

2.3.2. Wharton's Jelly addition

WJ 2.5 % (w/v) was prepared in 0.5X PBS. Then, the WJ solution was incorporated into the thermosensitive hydrogel formulation to a final concentration of 0.5 % (w/v).

2.4. Product characterization

SA/FA-CS and the thermosensitive hydrogel underwent vacuum drying, using a laboratory desiccator at room temperature until

dry powder was obtained. Dry powder samples were employed for product characterization through amine content determination. For FTIR and NMR analysis, samples were lyophilized at −80 °C and 0.007 mbar for 24 h (Lyophilizer HT 40, Beijer Electronics).

2.4.1. Amine content determination

The quantification of free amine content in the functionalized chitosan products was determined by ninhydrin assay using the modified method reported by Curotto and Aros in 1993 [27]. SA/FA-CS was dissolved in 1 % (v/v) acetic acid, through 30 s of vortexing. Then 0.05 mL of 4 M acetate buffer (pH 5.5) and 0.2 mL of ninhydrin solution (50 mg/mL in DMSO) were added to the sample solution (0.05 mL) and mixed. The reaction solution was heated to 100 °C for 20 min, then cooled to 25 °C and immediately placed into a 96-well plate. The absorbance was measured at 570 nm with a microplate spectrophotometer (FLUOstar Omega, BMG Labtech) and the obtained data was correlated with unmodified CS. The percentage of amine functionalization was indirectly calculated and relativized from the amine content determination, considering LMw CS as the 100 % of amino groups.

2.4.2. FTIR

Infrared spectra were recorded using a Thermo Nicolet Avatar 360 FTIR System. Before analysis, the samples underwent lyophilization, followed by grinding with KBr powder. These prepared samples were then pressed into disc pellets for thorough analysis. The infrared spectra were scanned at room temperature over the range of 4000 to 400 cm^{-1} in% transmittance mode, employing 32 scans and a resolution of 4.0. The spectra were analyzed in the OMNIC 7.1 software (Thermo Fisher Scientific).

2.4.3. NMR

Solid-state ^{13}C NMR spectra of functionalized CS were obtained using a Bruker Avance III WB400 spectrometer with 4 mm zirconia rotors spun at magic angle in N_2 at 10 kHz. Cross-polarization ^{1}H–^{13}C spectra were measured using a ^{1}H $\pi/2$ pulse length of 3 µs, with a contact time of 3 ms, and spinal64 proton decoupling sequence of 5.3 µs pulse length.

Liquid-state ^{1}H NMR spectroscopy was used to analyze genipin crosslinked products. The chemical shift region from 0 to 200 ppm or 0 to 9 ppm is shown for ^{13}C or ^{1}H analysis, respectively.

2.4.4. Elastic modulus

Uniaxial unconstrained compression tests were performed using a Nano Bionix Testing System (MTS). The hydrogels were elaborated with a cylindrical shape of 12 mm diameter and 5–8 mm height. Compression was performed with a 500 mN load cell between two parallel plates and a compression rate of 0.03 mm/s and 5 Hz of oscillatory frequency. The elastic modulus was calculated employing the stress–strain curves.

2.5. In vitro *biocompatibility and migration capacity*

2.5.1. Cell culture

MSCs from expanded adipose tissue (eASCs) were obtained from the laboratory's cell collection. Cells were cultured in 10 % FBS supplemented DMEM-F12 with 1 % (v/v) of Anti-Anti at 37 °C and 5 % CO_2. Cells were seeded in T75 tissue culture flasks until 90 % confluence was obtained and then they were seeded into well plates. Phenotype characteristics, clonic capacity, and stem cell differentiation biomarkers of eASCs are described by Gomez-Pinedo et al. [28]. iPS-OPCs were obtained from Celprogen (Netherlands). Cells were cultured in an OPC-specific medium at 37 °C and 5 % CO_2. After defrosting, cells were seeded into special T75 flasks, and cell culture-treated T75 flasks (Corning) were employed for further passages.

For 2D cell culture, 20,000 cells were seeded directly into the wells of a plate (96-well cell culture treated, Nunc) for their adhesion to the plastic surface. On the other hand, for 3D cell culture, 50,000 cells were homogeneously seeded into the thermosensitive hydrogel formulation and then placed into the wells (24-well cell culture treated, Nunc). For cell culture purposes, SA/FA-CS was sterilized by exposure to UV light followed by immersion in 70 % ethanol (0.22 µm filtered) and washed three times. Reaction buffer, 0.5X PBS for WJ preparation, and DMSO were 0.22 µm filtered before formulating the thermosensitive hydrogel.

2.5.2. Transfection with plasmid pcDNA-P2A-EGFP

iPS-OPCs were transfected with plasmid pcDNA3.2-P2A-EGFP (Figure S1). The vector was provided by Professor Ricardo Madrid, Faculty of Biology, Complutense University of Madrid, Madrid, Spain. Following the manufacturer's instructions, the transfection protocol was performed using the Lipofectamine 3000 transfection kit (Invitrogen). A concentration of 1 µg/µL of plasmid was employed. Cells were incubated at 37 °C and 5 % CO_2 for 48 h until harvested. EGFP-expressing iPS-OPCs (EGFP-iPS-OPCs) were incorporated into the thermosensitive hydrogel formulation before the intranasal administration.

2.5.3. Cell viability assay

An MTT-based *in vitro* toxicology assay kit (Sigma, Saint Louis, USA) was carried out for the biocompatibility evaluation, employing 24 h-cultured eASCs in 2D. Cells were incubated for 24 h at 37 °C and 5 % CO_2 in direct contact with a 4 × 4 mm slice of hydrogel, ECM-gel®, or 10 % (v/v) DMSO. The resulting absorbance was measured with a microplate spectrophotometer (FLUOstar Omega, BMG Labtech) at 590 nm, and the background was settled at 690 nm.

The Live/Dead kit was employed to observe cell viability after 24 h of direct contact with hydrogels. The results of 3D cultured cells were observed by confocal microscopy (Olympus, AF 1000) at excitation wavelengths of 488 nm and 546 nm. For the Live and Dead quantification, 2D cell culture was performed over hydrogel-pretreated 96-well culture plates (50 µL of hydrogel incubated for 24 h at 37 °C and 5 % CO_2 before inoculation). Plates were analyzed with a spectrophotometer (FLUOstar Omega, BMG Labtech) at 485/520 nm (excitation/emission) to measure the fluorescence of viable cells and at 544/520 nm (excitation/emission) for unviable cells.

For the graphic representation, the results were relative to the viability obtained from cells cultured in DMEM (2D) or ECM-gel® (3D) without additional material (100 % viability).

2.5.4. In vitro *migration assay*

The *in vitro* migration capacity of iPS-OPCs was evaluated using Chemotaxis µ-slides (Ibidi), where vascular endothelial growth factor (VEGF; 10 ng/mL) was employed as the chemoattractant on the right side of the slot. The instructions of the supplier for 3D gel matrices were followed for the assay implementation. However, live cell imaging was not executed, and endpoints were done instead at 0, 24, and 48 h of cell culture.

2.5.5. In vitro *iPS-OPCs stability*

iPS-OPCs were 2D cultured at 37 °C and 5 % CO_2 in direct contact with a 4 × 4 mm slice of hydrogel for up to 72 h. Every 24 h, cells were fixated in a 4 % (v/v) PFA and 7 % (w/v) sucrose PBS solution. Immunocytochemistry was carried out employing the primary antibodies: Ki67 (MA5-14520, 1:250), 8-OHdG (AB5830, 1:200), TERT (PA5116024; 1:100), c-MyC (13-2500, 1:500), PDGFR alpha (AB203491, 1:500), and RIP (MAB1580–1, 1:250), which were incubated overnight at 4 °C. Secondary antibodies: Alexa Fluor 488

(ab150073, 1:500), Alexa Fuor 555 (ab150130, 1:500), and Cy3-AffiniPure (715-165-150, 1:500) were incubated at room temperature for 2 h under light protection. Confocal microscopy (Olympus, AF 1000) was used for image obtention. Three different spots from the well were visualized for each marker and image obtention. ImageJ was employed for intensity measurement (integrated density), where ten aleatory cells were analyzed per image.

2.6. In vivo *retention time and migration capacity*

2.6.1. Animals

A total of ten male Athymic Nude NU(NCr)-Foxn1nu mice (Charles River Laboratories), 9 months old, were employed for the nasal retention time assay. Mice were kept in shared ventilated cages under controlled conditions, with access to food and water *ad libitum*, at the animal facilities of the Hospital Clínico San Carlos. The minimum number of animals necessary to obtain and replicate the results was used, under the current regulations of animal experimentation. All procedures were carried out by the regulations of the European Economic Community, 2010/63 / EU regarding the protection of animals for scientific purposes (Official Gazette of the Union of October 20, 2010, L 276/33), in force at the national level since February 2013, through Royal Decree 53/2013 of February 1st, 2013, and under the supervision of the Local Committee of Bioethics and Animal Welfare of our hospital and the Community of Madrid (PROEX: 002.3/22).

2.6.2. Intranasal administration

Mice were anesthetized through the intraperitoneal injection of ketamine/medetomidine (75/0.5 mg kg^{-1}; Pfizer/Ecuphar). For intranasal administration, mice were held on their left side and 10 µL of the thermosensitive hydrogel were gradually released into the right nostril. Then, the animals were placed face-up over a heated bed for 30 min. Anesthesia was reverted with Antisedan (1 mg kg^{-1}; Ecuphar) and mice were returned to their cages.

2.6.3. Histology

After 24, 48, 72 h, and 96 h of intranasal administration, animals were anesthetized, and, after perfusion with 4 % (v/v) buffered paraformaldehyde (0.1 M PBS), their heads were removed, and the brain and snout were extracted for further processing. Snouts were directly incubated in an aqueous mounting medium (FluorSave™ Reagent, Millipore) with Wheat Germ Agglutinin Alexa Fluor 647 (Invitrogen; 1:2000) and Dapi (1:1000 BioLegend). Brains were submerged in 4 % paraformaldehyde (PFA) solution in PBS until processed for cryoprotection in buffered Sacarose 30 % and inclusion in NEG-50™ (Thermo Scientific) and freezing at −20 °C for the sections obtention with a cryostat (Leica CM 1950). Brain sections of 30 µm thickness were incubated overnight with Human Nuclei antibody (1.5 µg/mL, Abcam) or for 2 h at room temperature with GFP-Dylight 488 (1:5000, Rockland Immunochemicals) conjugated secondary antibodies, also DAPI (1:2000, BioLegend) and DRAQ5 (1:5000, Life Technologies) were employed as nuclei labels. Images were obtained with a confocal microscope (Olympus, AF 1000) or an epifluorescence microscope (Olympus, BX53 LED).

2.7. Statistical methods

The statistical program GraphPad Prism v.8.0.1 was employed for data analysis and graphical representation of results. One-way analysis of variance followed by Sidak's or Dunnett's multiple comparisons test was used to draw comparisons between groups. 2-way ANOVA with Sidak's multiple comparisons was employed for the quantified intensity density of OPCs and oligodendrocyte markers in confocal images from different culture times. All data are expressed as the mean and standard error or the mean (SEM). The criterion for statistical significance was $p < 0.05$.

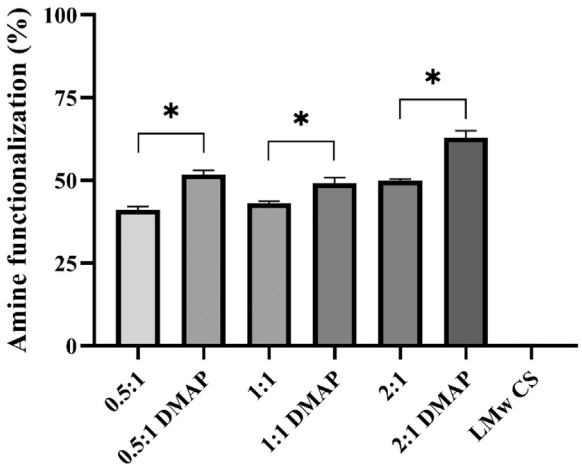

Fig. 2. Effect of the addition of DMAP catalyst on amine functionalization with succinic acid at different proportions. Graphical representation of the percentage of CS amines that are functionalized when different SA:CS ratios (0.5:1, 1:1, and 2:1) are employed in the Step 1 reaction, without or with DMAP catalyst. The amine functionalization represents the amino groups in CS that grafted SA. A significant increase in amine functionalization is indicated for each ratio when the DMAP catalyst is added to the reaction. Bars correspond to the mean + SEM.

3. Results

3.1. Chitosan functionalization

3.1.1. Effects of substituent concentration on functionalized chitosan

A first assay was performed to synthesize SA-CS (LMw) with different SA:CS's free amine molar ratios, with or without the addition of DMAP catalyst. The amine functionalization degree of the products increased significantly for the SA:CS ratios of 0.5:1, 1:1, and 2:1 when the DMAP catalyst was added (p-value < 0.0001, = 0.0101, and < 0.0001, respectively) (Fig. 2). The highest amine functionalization degree was 63 ± 2.1 % (SA:CS ratio of 2:1 with DMAP), despite doubling the molar concentration of free amines in CS (Table S1).

In contrast to unmodified CS, all SA-CS products were soluble in 1X PBS at pH 7.2, indicating that 39–50 % SA substitution degrees increased their water-solubility (p-values < 0.0001; Figure S2).

To achieve a low viscosity while keeping free amines, SA-CS was synthesized with the addition of DMAP with a SA:CS ratio of 1:1. A following Step 2 reaction was performed employing FA as the substituent, which was carried out with a FA:CS molar ratio of 0.25:1. The SA/FA-CS product presented an amine substitution of 68.4 ± 0.22 %, which is significantly higher than the obtained from the Step 1 reaction (49 ± 1.79 %; p-value < 0.0001), indicating a 19 % grafting of FA through amide bonds. The SA/FA-CS product with a SA:FA:CS ratio of 1:0.25:1 with DMAP addition, was used as starting material for further assays.

3.1.2. Ferulic and succinic acid-functionalized chitosan characterization

The ^{1}H NMR spectrum of SA/FA-CS in solution confirms the functionalization of CS (LMw) with both FA and SA (Fig. 3A). The new signal at 2.4 ppm corresponds to CH_2 from SA, which has been also reported for the succinylated CS [29]. Additionally, other new signals appear at 6.36 and 7.32 ppm corresponding to C=C of FA, as well as the signals at 6.79, 6.99, and 7.11 ppm correspond-

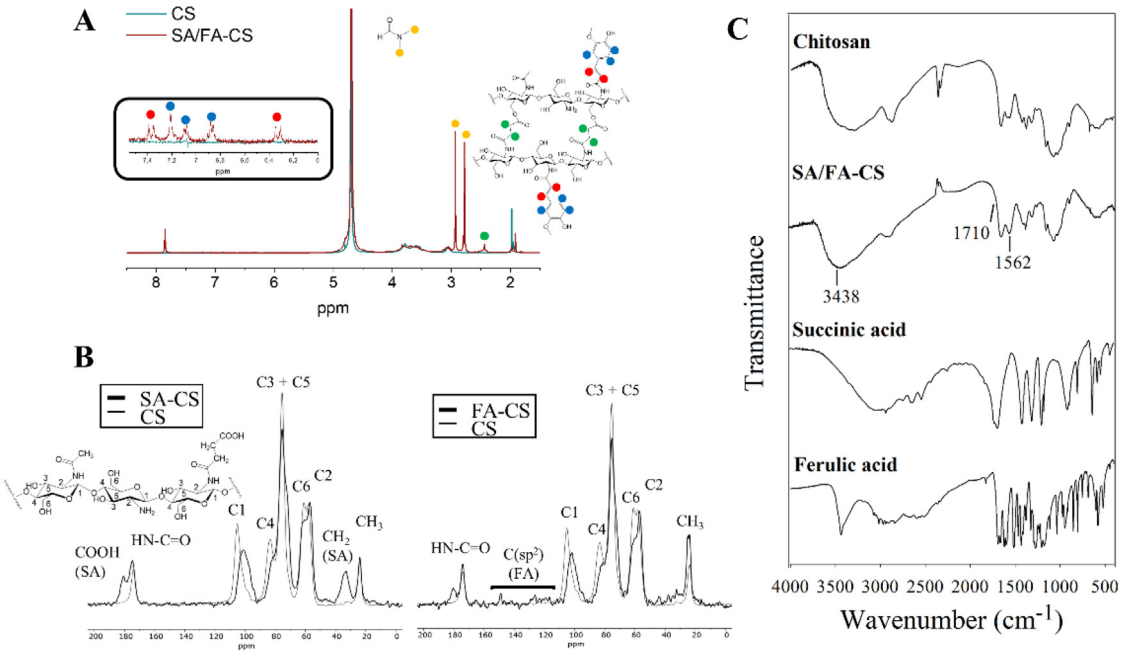

Fig. 3. Functionalized chitosan characterization. ^{1}H NMR of SA/FA-CS (A). CP-MAS-^{13}C NMR spectra of SA-CS and FA-CS (B). FTIR spectra of chitosan, SA/FA-CS, succinic acid, and ferulic acid (C).

ing to the aromatic ring of the FA (Fig. 3A inset) [30]. However, the need to use D_2O for this spectrum hampers the detection of mobile protons, such as those of the amide group. The spectrum also reveals the presence of an important amount of DMF (signals of the two methyl groups at 2.73 and 2.98 ppm; Fig. 3A), which remains adsorbed on the modified CS, and it would mask the carbonyl groups in ^{13}C NMR. Hence, the ^{13}C analysis was carried out in solid phase by CP-MAS-NMR, taking advantage of the lack of signal due to the fast relaxation in the highly mobile adsorbed DMF molecules.

The functionalization with SA and FA was studied separately on SA-CS and FA-CS (Fig. 3B). SA-CS showed the incorporation of the substituent through the presence of methylene groups (-CH_2-) at 33 ppm. An increase of the C=O signal at 174 ppm indicated the formation of new amide bonds (however, this signal could also correspond to an ester bond), and an additional signal appeared at 180 ppm, corresponding to free carboxylic groups. The C(sp^2) signals of FA-CS in the 115–150 ppm range are not clearly visible; however, the modification of the CS chain is analogous to the changes observed in the SA-CS spectrum, with slight but significant downfield shifts of most of the CS signals. Therefore, it can be deduced that the content of FA must be quite similar, and the reason for the much lower signals must be due to the worse cross-polarization in the case of sp2 carbons of FA.

The most notorious changes observed by FTIR (Fig. 3C) after CS functionalization with SA and FA are the increase of the peak at 3438 cm^{-1}, attributed to the characteristic peak of OH- from FA, and the increase of a peak at 1562 cm^{-1}, characteristic of N–H bending of amide II bonds [31]. The presence of DMF, as demonstrated by ^{1}H NMR, makes difficult the interpretation of the C=O region of the IR spectrum, mainly the detection of the possible formed amides. The small shoulder at 1710 cm^{-1} may be assigned to free COOH groups of grafted SA [21], in agreement with the signal at 180 ppm in ^{13}C CP-MAS-NMR. When DMAP is added to the reaction, an additional very small shoulder appears at 1730 cm^{-1} (Fig. S3), which may be attributed to ester bonds formed between the carboxylic groups of SA or FA and the hydroxyl groups of CS [23,32].

Table 1
Gelation time of the thermosensitive hydrogel formulations at 37 °C.

Molecular weight	pH	SA/FA-CS (%)	Genipin / DMSO (%)	Gelation time (min)
MMw	7.2	12	0.05 / 5	10
		8		15
		4		20
			0.1 / 10	30
			0.02 / 2	>30
		2		15
				20 *
LMw	6.5		0.01 / 1	15 *
				15 *
MMw				10 *

Although the gelation time was determined through the tube tilting, the characteristic blue color from genipin crosslinking began to be perceptible to the human eye after an hour of incubation at 37 °C.
* Selected formulations.

3.2. Thermosensitive hydrogel formulation

3.2.1. Gelation time

Different gelation times were obtained with the variations in the concentrations of MMw SA/FA-CS or genipin dissolved in DMSO (Table 1). A higher concentration of SA/FA-CS resulted in shorter gelation time, however, the viscosity increased and difficulted the obtention of a homogeneous hydrogel. On the other hand, the increase in the concentration of genipin and its cosolvent did not traduce in a shorter gelation time. The formulations with high concentrations of genipin and its cosolvent (0.1/10 and 0.2/20), resulted in dense products with poor swelling capacity. The formulation composed of 2 % of SA/FA-CS and 0.1/10 % of genipin/DMSO was evaluated also employing SA/FA-CS of LMw and at pH 6.5, where all products presented <20 min gelation times.

3.2.2. Hydrogel characterization

The selected formulations gave place to soft hydrogels (Fig. S4). The elastic modulus values were calculated from the exponential increment of the stress-strain curves of compression tests (Fig. S5).

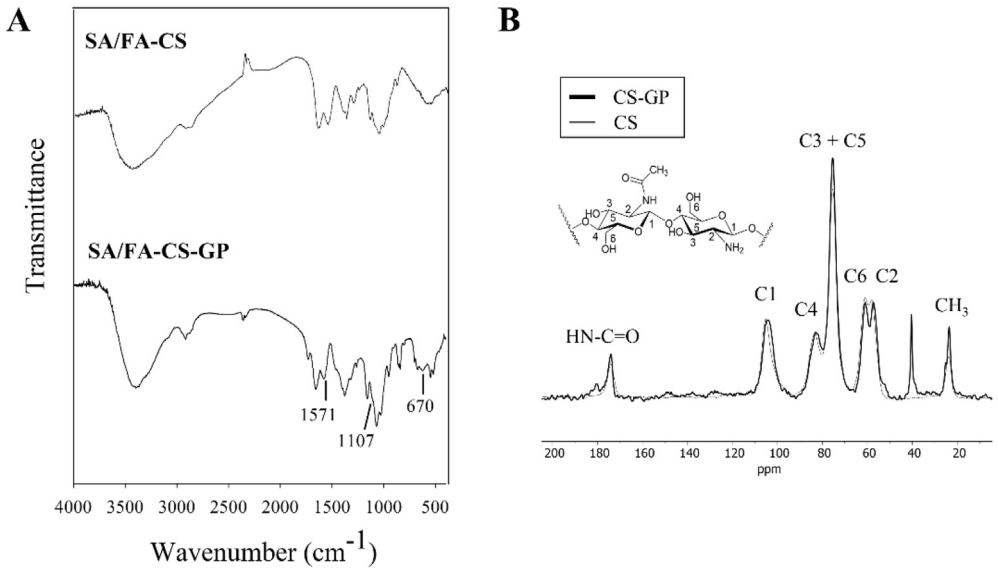

Fig. 4. Chemical characterization of the thermosensitive hydrogel formulation. FTIR spectrum of LMw SA/FA-CS and SA/FA-CS after crosslinking with GP (SA/FA-CS-GP) and curing for 24 h at pH 7.2 (A), and CP-MAS-^{13}C NMR spectrum of CS crosslinking with GP (B).

The elastic modulus of both hydrogels, LMw and MMw at pH 7.2, was near 1 kPa.

The FTIR spectrum of SA/FA-CS crosslinked with genipin (SA/FA-CS-GP) presented a wide band ranging between 3600 and 3000 cm^{-1} due to the partially overlapped O–H and N–H stretching vibrations. After functionalization, this signal is stretched, which can be attributed to a reduction in the number of free O–H groups, resulting in a decreased density of hydrogen bonds. An increase of the peak at 1571 cm^{-1} was also observed, characteristic of N–H in-plane bending of secondary amide, probably due to the amide bond formation between CS and genipin, and a small peak at 670 cm^{-1} due to N–H out-of-plane bending of secondary amides. The new peak at 1731 cm^{-1}, corresponding to C=O stretching of an ester probably corresponds to unreacted genipin residues [33]. The small signal at 1461 cm^{-1} corresponds to CH_3 bending of a methyl ester. The small shoulder at 1107 cm^{-1} is assigned to the C–N stretch of the tertiary aromatic amine of the crosslinked genipin nitrogen iridoid that is bound covalently to CS. The new peak at 838 cm^{-1} results from the bonds in the polymerized genipin [34,35] (Fig. 4A).

The CP-MAS-^{13}C NMR spectra of CS (MMw) after crosslinking with GP did not show the same modification of the CS chains as observed for the functionalization products. The only clear new signal at 40 ppm cannot be assigned to genipin and is probably due to DMSO, used as a cosolvent in the formulation. In this way, CP-MAS-^{13}C NMR was not able to locate structural changes related to genipin crosslinking. Although there are some reports of crosslinking with genipin, the structure of genipin is not detectable in the NMR spectra [36–39] (Fig. 4B).

3.3. In vitro *biocompatibility, cell migration capacity, and cell stability*

3.3.1. In vitro *biocompatibility of the thermosensitive hydrogel*

The *in vitro* biocompatibility evaluation in 2D-cell culture of eASCs compared SA/FA-CS-GP of LMw and MMw at pH 6.5 and 7.2 (Fig. 5A). The four formulations of the hydrogels exhibited good biocompatibility, resulting in >95 % viability. Although no statistically significant differences were observed, there was a tendency for increased cell viability with the LMw formulation at pH 7.2. However, in 3D-cell culture, cell viability decreased, particularly with hydrogels formulated at pH 6.5 (Fig. 5B).

To enhance cell viability in the thermosensitive hydrogels at pH 7.2, the addition of WJ was evaluated in a 2D-cell culture assay to assess its cytoprotective effect in the presence of a cytotoxic agent (5 % DMSO) (Fig. 5C). The results indicated that adding 0.5 % (w/v) of WJ increased eASCs viability from 75 % to 101 % under cytotoxic conditions. In non-cytotoxic conditions, WJ increased cell proliferation by 30 %.

The impact of WJ addition to the thermosensitive hydrogel formulations was evaluated on a 3D-cell culture of eASCs. Live and Dead labeling indicated high cell viability, maintained even 72 h post-inoculation (Fig. 5D).

In 2D-cell culture, iPS-OPCs on hydrogel-treated wells showed viability results similar to those of eASCs. The thermosensitive hydrogel of LMw and MMW showed 99.7 ± 0.12 % and 99.2 ± 0.12 % of iPS-OPCs viability, respectively, using ECM-gel as a control of 100 ± 0.39 % viability.

The addition of WJ caused a 5-minute delay in the gelation time, resulting in a final gelation time of 20 min for LMw and 25 min for MMw thermosensitive hydrogel formulations.

3.3.2. In vitro *cell migration*

iPS-OPCs were observed outside the inoculation channel after 24 h of incubation, with a higher concentration on the chemoattractant side of the slot (Fig. S6). After 48 h, cells reached farther zones, particularly those in the LMw SA/FA-CS-GP (data not shown). Therefore, further assays used the LMw SA/FA-CS for hydrogel formulation. The results indicate that the cells retain the capacity to migrate out of the hydrogel *in vitro*.

3.3.3. *iPS-OPCs stability after contact with the LMw thermosensitive hydrogel*

Direct contact of the LMw thermosensitive hydrogel in 2D cultured iPS-OPCs did not significantly affect cell proliferation (Ki67), oxidative DNA damage (8-OHdG), telomerase (TERT), or c-MyC expression for up to 72 h (Fig. S7). These findings suggest that the hydrogel does not induce oxidative or tumorigenic responses. The OPC marker (PDGFRα) of the hydrogel-contacting cells was significantly increased (p-value = 0.0035) in hydrogel-contacting cells at 72 h compared to the control group (Fig. 6), which showed a significant decrease from 24 to 72 h of cell culture (p-value = 0.0207).

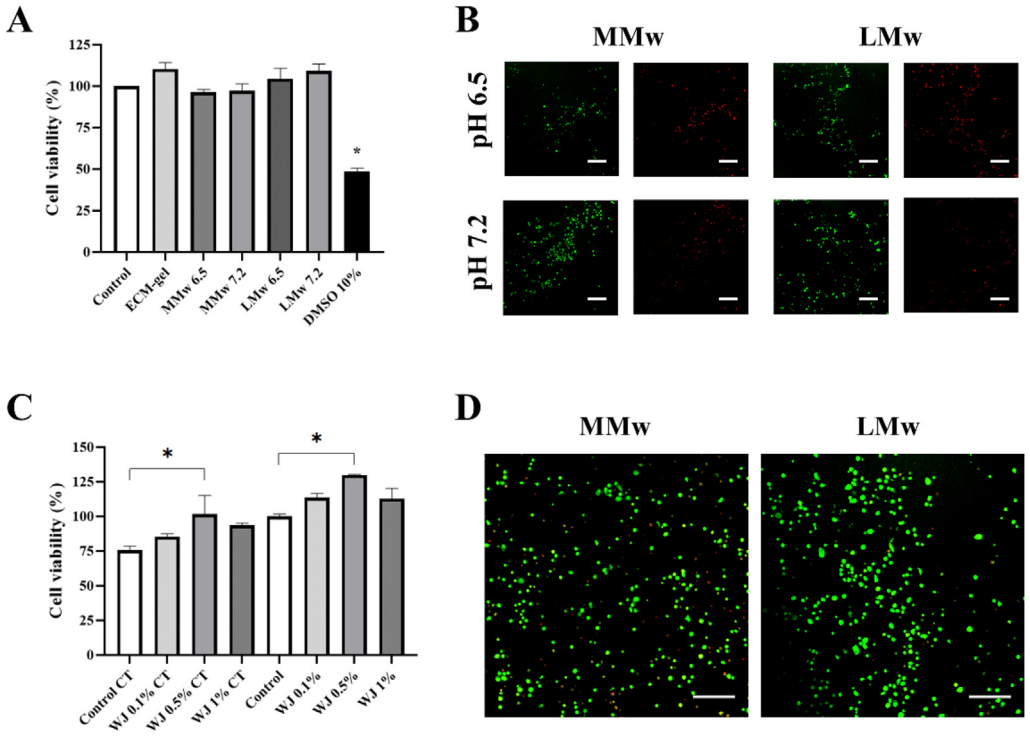

Fig. 5. *In vitro* biocompatibility of thermosensitive hydrogels. Cell viability of eASCs with SA/FA-CS-GP of MMw or LMw, at pH 6.5 or 7.2, in 2D- (A) and 3D-cell culture (B). *In vitro* evaluation of the cytoprotective effect of Wharton's Jelly (WJ) on 2D-cultured eASCs in a cytotoxic media (CT; DMSO 5 %) or normal conditions (C); and representative images of 3D-cultured eASCs into SA/FA-CS-GP of MMw and LMw at pH 7.2 supplemented with WJ (D). Images B and D were taken through confocal microscopy. The scale bars correspond to 200 µm. Bars consist of mean + SEM.

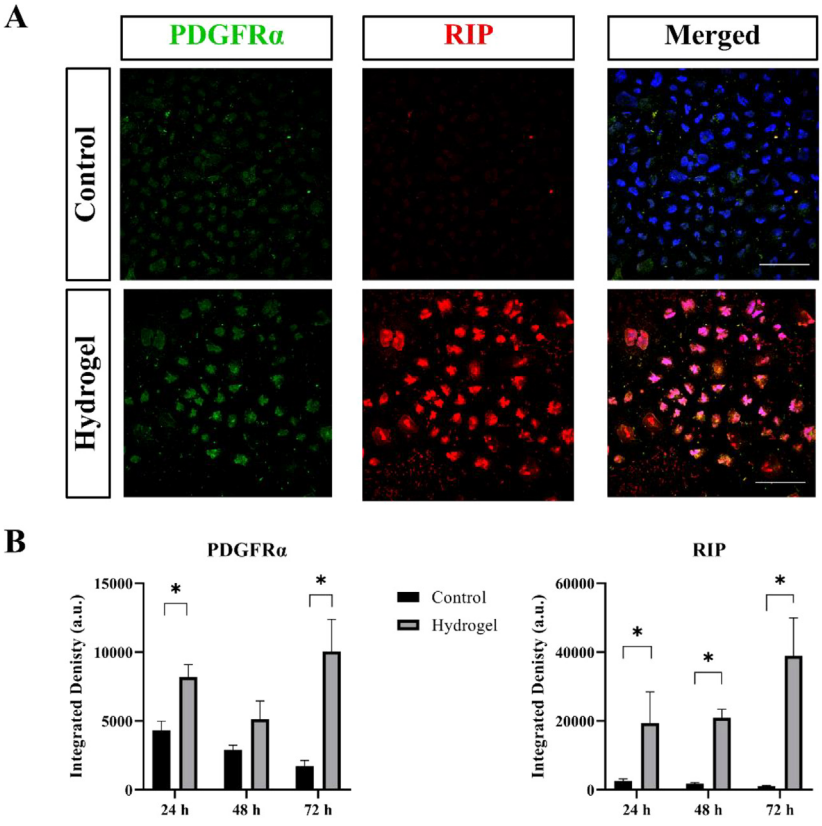

Fig. 6. Effect of the thermosensitive hydrogel on the expression of OPC and oligodendrocyte markers. (A) Confocal microscopy images of 2D-cultured iPS-OPCs for 72 h under normal conditions (Control) or direct contact with the thermosensitive hydrogel of LMw at pH 7.2 (Hydrogel). Images show the OPC marker (PDGFRα, green), oligodendrocyte marker (RIP, red), and cell nuclei (Draq, blue). The scale bar corresponds to 50 µm. (B) Quantitative analysis of the integrated density for PDGFRα and RIP expression after 24, 48, and 72 h of cell culture. Bars correspond to mean + SEM.

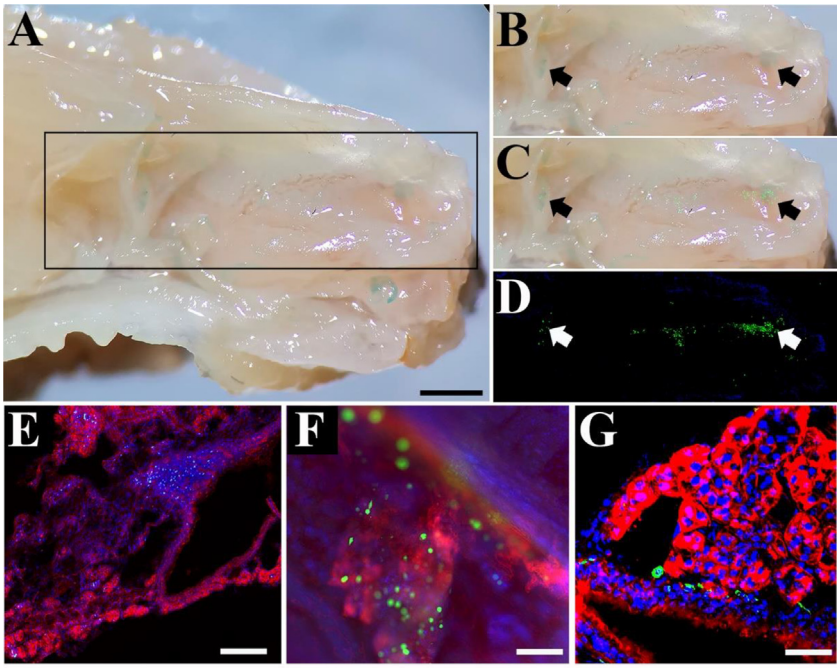

Fig. 7. EGFP-iPS-OPCs and thermosensitive hydrogel (LMw) distribution after 24 h of intranasal administration in mice. Images show representative photography of the mice snout (A), where arrows point to the hydrogel's adhesions to nasal mucosa (B), a merged image of fluorescent EGFP-iPS-OPCs (green) that matches with the hydrogel distribution (C), and a fluorescence microscopy image of the EGFP-iPS-OPCs (green) and cell nuclei (DAPI, blue) (D). Fluorescence microscopy images show EGFP-iPS-OPCs contained in the hydrogel at the nasal chamber after 24 h of intranasal administration in an x-y plane (E) or x-y-z plane (F). Confocal microscopy image shows iPS-OPCs (Human nuclei, green), cell nuclei (DAPI, blue), and hydrogel and cell membrane (WGA, red) after 72 h of intranasal administration, in an x-y plane (G). The scale bars correspond to A, B, C: 800 µm; E: 400 µm; F: 100 µm; and G: 40 µm.

Additionally, RIP expression was significantly higher in cells after hydrogel contact compared to the control group.

3.4. In vivo *cell retention and cell migration capacity after intranasal administration*

After 24 h of the intranasal administration, the EGFP-iPS-OPCs contained in the LMw hydrogel were found distributed alongside the nasal atrium, from the turbinate to the olfactory epithelium (Fig. 7A–D). After 96 h, some cells were found still attached to the nasal epithelium, and traces of hydrogel were visible (data not shown).

After 24 h of intranasal administration, iPS-OPCs were found mainly contained in the hydrogel, distributed in different areas of the nose-to-brain route, including the nasal vestibule, ostium, and nasal chamber, which is the anatomical place where inspired air is heated (Fig. 7C–F). 72 h post-administration, by the interest of this study, cells were found mainly released in the nasal turbinates, olfactory recess, and nasal epithelium, where the nose-to-brain journey begins (Fig. 7G). The presence of cells and the progressive depletion of the hydrogel 48 h post-administration indicated that cells were viable and capable of going forth outside the hydrogel to migrate toward the brain parenchyma (Figure S8).

4. Discussion

In this work, a thermosensitive hydrogel is formulated as a vehicle to improve nose-to-brain cell therapy. For this purpose, CS was functionalized with FA and SA via carbodiimide-mediated reaction. The functionalization improved the solubility at physiological pH and enhanced its potential as a base material for the thermosensitive hydrogel formulation. The formulated hydrogel exhibited thermogelling properties, mucoadhesive capacity, and biocompatibility with MSCs and iPS-OPCs, which are critical for improving cell survival and retention in the nasal cavity. This was confirmed *in vivo* following intranasal administration of iPS-OPCs in healthy athymic mice.

Changes in the molecular structure of functionalized CS were confirmed using FTIR and NMR spectra after grafting both SA and FA. Notably, the NMR spectra showed modifications of the CS chains, with most signals shifting to lower chemical shifts (higher magnetic field) due to SA grafting. Similar effects have been observed in previous studies on crosslinking CS [29,40], although the exact cause of this shift remains undetermined. The low reaction efficiency observed may be attributed to the mild conditions used (30 °C) to preserve CS integrity. While it is crucial to maintain free amines for crosslinking with genipin, careful washing is necessary to remove non-binding residues, suggesting the potential for improving functionalization efficiency. Elevated temperatures (*e.g.* 60 °C) could increase chain reactivity and motility, thus favoring higher grafting efficiency [30], albeit at the risk of compromising CS integrity. Future research could explore alternative strategies for covalently binding carboxylic moieties of SA and FA to CS to enhance functionalization efficiency [19,20]. Consistent with findings here, carbodiimide-based functionalization reactions using low molar ratios <0.5:1 of carboxylic acid:CS's free amine, at low or mild temperatures, have achieved <80 % substitution [41,42]. The addition of DMAP overcame amine substitution to some extent, yet also facilitated ester bond formation with primary hydroxyl groups of CS, as previously reported [23]. This highlights the challenge in crosslinking polymeric chains via dicarboxylic acids in less substituted products, despite retaining more free amines for genipin reaction, leading to higher viscosity and pipetting difficulties that may complicate intranasal administration. Increased viscosity in CS has been associated with higher molecular weight [11], which typically increases with substituent grafting; however, viscosity tends to initially rise with small substitution degrees and decrease at higher levels [43–45].

Solubility is a critical factor in achieving homogeneous hydrogels. Unmodified CS is soluble in acidic media, but a low pH in the hydrogel formulation would not be suitable due to the importance of maintaining cell viability. Therefore, SA/FA-CS demonstrated superior applicability for formulating the thermosensitive hydrogel. The improved solubility of functionalized CS can be attributed to the incorporation of SA's hydrophilic carboxylic groups into its molecular structure [46], a phenomenon previously observed with different carboxylic acids grafted onto CS [47]. Additionally, solubility can indicate a low rate of SA crosslinking (Fig. 1). The presence of free acids and amines contributes to the formation of zwitterionic species (-COO^- and -NH_3^+) that enhance the interaction between polymeric chains and water. Furthermore, the opposite charges in functionalized CS may facilitate the interaction of the vehicle with mucin and the epithelium in the nasal cavity, thereby promoting mucoadhesion.

Migration of intranasally administered cells into brain parenchyma has been reported to occur from 1 h post-administration [48] up to several hours later [49]. Shorter times are achieved with prior administration of permeability enhancers (*e.g.* hyaluronidase). Although some authors have noted cells remaining in the nasal cavity for hours, their viability is compromised by pH, enzymes, and immune responses. Genipin was incorporated into the vehicle formulation to achieve a thermo-responsive short gelation time within <30 min, providing a favorable microenvironment for cell viability and retention in the nasal cavity. The thermogelling time of the hydrogel can be shortened with increased SA/FA-CS concentration, as closer proximity of polymeric chains favors genipin crosslinking between free amines, forming a three-dimensional matrix [26]. However, high concentrations of SA/FA-CS (4 %, 8 %, and 12 %) also resulted in viscous formulations and heterogeneous hydrogels. Therefore, 2 % of SA/FA-CS was chosen for evaluating different genipin concentrations. Despite the slightly faster gelation with 0.02 % genipin, 0.01 % was selected to maintain more free amines and preserve the hydrogel's bioactivity. Small pH changes (4.0–5.5) have been reported to significantly affect CS gelation and genipin crosslinking [26], although this was not observed in our work at pH 6.5 and 7.2. A pH of 6.5 was considered for the vehicle formulation to minimize nasal epithelium irritation, as intranasal formulations are recommended within a pH range of 4.5–6.5 [50]. However, pH 6.5 hydrogels adversely affected cell viability. Given the priority of preserving cell integrity for this application, pH 6.5 formulations were discarded in favor of further assays at pH 7.2. Incorporating 0.5 % WJ showed a cytoprotective effect, enhancing cell viability in 3D OPC cultures. Unexpectedly, higher WJ concentrations (1 %) did not further increase cell viability, with or without cytotoxic media. Similar results have been reported where WJ-coated flasks enhanced cell proliferation and adhesion under shear stress [51], with optimal results observed at 0.5 % (w/v) WJ, increasing mitochondrial activity in umbilical cord MSCs. Moreover, media supplemented with WJ (2.5–50 % of humid extract) enhanced human endometrial stem cell proliferation after 24 h [52]. Besides its proliferative effects, WJ has been shown to preserve MSCs by delaying senescence [53], making it valuable in cell therapy design. Given these benefits, WJ can be incorporated into hydrogels designs for 3D culture and implantation, improving biomimetic properties and cytocompatibility as recently demonstrated in some WJ-containing hydrogels [54,55]. The glycosaminoglycans (GAGs) extract from WJ primarily comprises hyaluronic acid, and to a lesser extent, heparin and sulfated GAGs such as chondroitin sulfate, keratan sulfate, heparan sulfate, and dermatan sulfate [56]. Therefore, adding WJ to the vehicle formulation could lead to ionic interactions between GAGs and functionalized CS. The weak negative charges of hyaluronic acid may interact with the free amines in the SA/FA-CS, depending on their protonation at pH 6.5 and 7.2. CS amine protonation occurs at pH 6.5, but amino groups tend to remain partially protonated at neutral pH [57], potentially influencing the pKa values of modified CS during dissociation in aqueous systems [58]. Since it would be difficult to identify the interactions with GAGs in such a complex formulation, future studies should determine the pKa of SA/FA-CS to better characterize these interactions.

Once the vehicle's biocompatibility was confirmed, it was essential to assess its impact on cells, evaluating proliferation capacity, oxidative stress, genetic stability, and OPC differentiation. Significant differences were observed in both PDGFRα and RIP markers. PDGFRα signaling plays a crucial role in OPC proliferation, migration, and differentiation, while RIP (2′,3′-cyclic-nucleotide 3′-phosphodiesterase) is associated with early myelin expression and has long been used to identify oligodendrocyte lineage cells. Despite the rapid PDGFRα downregulation during differentiation, simultaneous expression of OPC and oligodendrocyte markers in cell culture has been reported [59], This phenomenon has been attributed to the *in vitro* inhibition of the differentiation of oligodendrocyte lineage cells into mature oligodendrocytes. However, this differentiation inhibition has not remained after cell implantation in animal models. Therefore, the differentiation capacity of stem cells needs to be corroborated in further *in vivo* studies with therapeutic purposes.

The intranasal administration of the iPS-OPCs was facilitated by the homogeneous and slightly viscous nature of the designed vehicle. The use of highly viscous formulations can cause dyspnea, while low viscosities can lead to the flow from the nasal cavity [60]. The mucoadhesive properties of CS-based formulations enhance the retention time of bioactive molecules in the nasal mucosa [61]. In this study, these properties are attributed to the positive and negative charges in the functionalized CS. The co-localization of the hydrogel with the fluorescence of EGFP-iPS-OPCs in the nasal cavity demonstrated that the hydrogel could retain cells for up to 72 h post-administration. Additionally, interactions between the administered cells and the nasal epithelium were observed, indicating that the cells maintained their viability and migration capacity. Since the cells and hydrogel were localized along the nasal atrium, a nose-to-brain migration from the respiratory and olfactory epithelium could be expected via the olfactory or trigeminal nerves [8]. The importance of mucopenetration in the olfactory region is crucial for nose-to-brain applications [15]. The capacity of CS-based hydrogels to open tight junctions and line the nasal epithelium has been previously reported [16]. Although this study did not evaluate the opening of epithelial junctions, a structural analysis of the nasal epithelium using epithelial markers such as cytokeratin AE1/AE3 and WGA, allowed us to observe no alterations in the nasal epithelium caused by the hydrogel formulation compared to the epithelium from the control group (see Fig. S9). On the other hand, the histological and immunohistochemical analysis demonstrated the presence of the administered iPS-OPCs near the cribriform plate, the olfactory bulbs, and cortical areas. This provides clear evidence that the biomaterial is a bioactive carrier with the ability to facilitate mucopenetration, making this biomaterial of great interest in cell therapy. This study introduces the application of hydrogels to improve nose-to-brain cell therapy for the first time, marking a significant advancement in enhancing delivery efficiency for future translational medicine approaches, not only for this cell type but also opening a range of possibilities for other neurological or vascular pathologies where cell therapy can have a significant impact.

The data obtained highlights several challenges that are beginning to be addressed. The first major challenge is translating the preclinical model into a clinical setting. This is particularly complex due to the notable differences between the nasal epithelium of rodents and humans. Therefore, one of the primary objectives

is to establish a clinical safety trial in humans focused specifically on evaluating the effects of the hydrogel on the human nasal epithelium. While no alterations are observed in the nasal epithelium of animals treated with hydrogel-containing cells, it is essential to confirm these findings in humans.

These data demonstrate that two distinct types of cell strains, eASCs and OPCs (of mesodermal and ectodermal origin, respectively), show clear evidence of a critical factor: shelf life. Under controlled storage conditions (humidity, physiological pH, and temperature), these cells remain viable for more than 72 h with a viability rate exceeding 85 % (data not shown). This finding is comparable to commercial preservation solutions such as HypoThermosol® FRS and SPS-1® (UW Solution). This viability and biocompatibility are essential for generating the hydrogel and ensuring there is enough time for its administration at various centers, even those located far apart, that produce cells and biomaterials.

In the animal studies involving intranasal administration and subsequent brain monitoring, the administered cells were successfully identified using transfected protein labels or specific immunohistochemistry markers. These cells were localized in areas known for the presence of quiescent endogenous OPCs, such as the corpus callosum, subventricular zone (SVZ), atrium, septum, and striatum. The research focuses on exploiting this therapeutic route, which holds significant potential because it does not require specialized training for administration, unlike stereotactic surgery. Furthermore, this approach allows for repeated dosing without apparent adverse effects. The hydrogel design is not limited to a single pathology or cell line; it has potential applications in other neurological diseases, such as stroke (using mesenchymal cells to modulate inflammation), Parkinson's disease (using dopaminergic cells from the carotid body or iPSCs), and glioblastoma multiforme (using genetically edited cells to target brain tumor stem cells). Additionally, our ongoing and unpublished studies suggest that the hydrogel could serve as a carrier for exosomes, offering a promising acellular therapy with significant therapeutic potential.

5. Conclusions

The functionalization of CS with SA and FA was shown to be a useful strategy to increase its applicability, increasing solubility at physiological pH exhibited thermogelling properties and good biocompatibility with MSCs and iPS-OPCs, demonstrating the potential for use in various neurological disorders. In addition to increasing residence time in the nasal cavity, the hydrogel provided a favorable environment for cell viability and migration capacity for up to 72 h. Future studies should track the biodistribution of cells in the brain and evaluate the use of the formulated hydrogel in different models of neurological disorders. This approach opens the possibility of enhancing the nose-to-brain cell delivery efficiency for future translational medicine approaches.

Funding

This work was supported by the Ministry of Science and Innovation, Spain [grant number AES, ISCIII PI21/00242]; and CONAHCYT-México [grant number 809831].

Declaration of competing interest

The authors declare that they have no known competing financial interests or personal relationships that could have appeared to influence the work reported in this paper.

CRediT authorship contribution statement

Doddy Denise Ojeda-Hernández: Writing – original draft, Investigation. **Susana Velasco-Lozano:** Resources, Investigation. **José M. Fraile:** Formal analysis. **J.C. Mateos-Díaz:** Visualization. **Francisco J. Rojo:** Formal analysis. **María Soledad Benito-Martín:** Validation. **Belén Selma-Calvo:** Formal analysis. **Sarah de la Fuente-Martín:** Formal analysis. **Marina García-Martín:** Validation. **María Teresa Larriba-González:** Validation. **Mercedes Azucena Hernández-Sapiéns:** Methodology. **Alejandro A. Canales-Aguirre:** Methodology. **Jordi A. Matias-Guiu:** Methodology. **Jorge Matias-Guiu:** Supervision. **Ulises Gomez-Pinedo:** Writing – review & editing, Funding acquisition.

Acknowledgments

The authors would like to thank Ricardo Madrid, Professor of the Faculty of Biology at the Complutense University, Spain for providing the plasmid. The authors thank Histocell S.L. for providing Wharton's Jelly. SV acknowledges ARAID for the funding.

Supplementary materials

Supplementary material associated with this article can be found, in the online version, at doi:10.1016/j.actbio.2024.09.002.

References

[1] S.I. Savitz, C.S. Cox, Cell-based therapies for neurological disorders — The bioreactor hypothesis, Nat. Rev. Neurol. 19 (2023) 9–18.
[2] H. Huang, A. Ramon-Cueto, W. El Masri, G.A. Moviglia, H. Saberi, H.S. Sharma, A. Otom, L. Chen, D. Siniscalco, A. Sarnowska, Chapter six - advances in neurorestoratology—current status and future developments, in: H.S. Sharma, L. Wiklund, A. Sharma (Eds.), International Review of Neurobiology, Academic Press, 2023, pp. 207–239.
[3] H. Huang, P.R. Sanberg, G.A. Moviglia, A. Sharma, L. Chen, D. Chen, Clinical results of neurorestorative cell therapies and therapeutic indications according to cellular bio-proprieties, Regenerat. Therapy 23 (2023) 52–59.
[4] W. Li, T. He, R. Shi, Y. Song, L. Wang, Z. Zhang, Y. Tang, G.Y. Yang, Y. Wang, Oligodendrocyte precursor cells transplantation improves stroke recovery via oligodendrogenesis, neurite growth and synaptogenesis, Aging Dis. 12 (2021) 2096–2112.
[5] S. Wang, J. Bates, X. Li, S. Schanz, D. Chandler-Militello, C. Levine, N. Maherali, L. Studer, K. Hochedlinger, M. Windrem, S.A. Goldman, Human iPSC-derived oligodendrocyte progenitor cells can myelinate and rescue a mouse model of congenital hypomyelination, Cell Stem Cell 12 (2013) 252–264.
[6] J. Sharp, J. Frame, M. Siegenthaler, G. Nistor, H.S. Keirstead, Human embryonic stem cell-derived oligodendrocyte progenitor cell transplants improve recovery after cervical spinal cord injury, Stem Cells 28 (2009) 152–163.
[7] Y.-T. Zhang, K.-J. He, J.-B. Zhang, Q.-H. Ma, F. Wang, C.-F. Liu, Advances in intranasal application of stem cells in the treatment of central nervous system diseases, Stem Cell Res. Ther. 12 (2021) 210.
[8] N. Villar-Gómez, D.D. Ojeda-Hernandez, E. López-Muguruza, S. García-Flores, N. Bonel-García, M.S. Benito-Martín, B. Selma-Calvo, A.A. Canales-Aguirre, J.C. Mateos-Díaz, P. Montero-Escribano, J.A. Matias-Guiu, J. Matías-Guiu, U. Gómez-Pinedo, Nose-to-brain: the next step for stem cell and biomaterial therapy in neurological disorders, Cells 11 (2022) 3095.
[9] S. Gänger, K. Schindowski, Tailoring formulations for intranasal nose-to-brain delivery: a review on architecture, physico-chemical characteristics and mucociliary clearance of the nasal olfactory mucosa, Pharmaceutics 10 (2018) 116.
[10] A. Kumar, A. Vimal, A. Kumar, Why Chitosan? From properties to perspective of mucosal drug delivery, Int. J. Biol. Macromol. 91 (2016) 615–622.
[11] I. Aranaz, A.R. Alcántara, M.C. Civera, C. Arias, B. Elorza, A. Heras Caballero, N. Acosta, Chitosan: an overview of its properties and applications, Polymers (Basel) 13 (2021) 3256.
[12] A. Harugade, A.P. Sherje, A. Pethe, Chitosan: a review on properties, biological activities and recent progress in biomedical applications, Reactive Funct. Polym. 191 (2023) 105634.
[13] D.D. Ojeda-Hernández, A.A. Canales-Aguirre, J. Matias-Guiu, U. Gomez-Pinedo, J.C. Mateos-Díaz, Potential of chitosan and its derivatives for biomedical applications in the central nervous system, Front. Bioeng. Biotechnol., 8 (2020) 389.
[14] K.P. Alcantara, N. Nalinratana, N. Chutiwitoonchai, A.L. Castillo, W. Banlunara, O. Vajragupta, P. Rojsitthisak, P. Rojsitthisak, Enhanced nasal deposition and anti-coronavirus effect of favipiravir-loaded mucoadhesive chitosan–alginate nanoparticles, Pharmaceutics 14 (2022) 2680.
[15] H. Gholizadeh, S. Cheng, M. Pozzoli, E. Messerotti, D. Traini, P. Young, A. Kourmatzis, H.X. Ong, Smart thermosensitive chitosan hydrogel for nasal delivery of ibuprofen to treat neurological disorders, Expert Opin. Drug Deliv. 16 (2019) 453–466.
[16] A. Khan, M. Aqil, S.S. Imam, A. Ahad, Y. Sultana, A. Ali, K. Khan, Temozolomide loaded nano lipid based chitosan hydrogel for nose to brain delivery: characterization, nasal absorption, histopathology and cell line study, Int. J. Biol. Macromol. 116 (2018) 1260–1267.

[17] N. Vasquez-Martínez, D. Guillen, S.A. Moreno-Mendieta, S. Sanchez, R. Rodríguez-Sanoja, The role of mucoadhesion and mucopenetration in the immune response induced by polymer-based mucosal adjuvants, Polymers (Basel) 15 (2023) 1615.
[18] P. Mura, F. Maestrelli, M. Cirri, N. Mennini, Multiple roles of chitosan in mucosal drug delivery: an updated review, Mar. Drugs 20 (2022) 335.
[19] L. Nicolle, C.M.A. Journot, S. Gerber-Lemaire, Chitosan functionalization: covalent and non-covalent interactions and their characterization, Polymers (Basel) 13 (2021) 4118.
[20] D.D. Ojeda-Hernández, A.A. Canales-Aguirre, J.A. Matias-Guiu, J. Matias-Guiu, U. Gómez-Pinedo, J.C. Mateos-Díaz, Chitosan-hydroxycinnamic acids conjugates: emerging biomaterials with rising applications in biomedicine, Int. J. Mol. Sci. 23 (2022) 12473.
[21] F. Gabriele, A. Donnadio, M. Casciola, R. Germani, N. Spreti, Ionic and covalent crosslinking in chitosan-succinic acid membranes: effect on physicochemical properties, Carbohydr. Polym. (251) (2021) 117106.
[22] R. Medimagh, H. Aloui, M. Jemli, H. Chaabane, F. Belkahla, K. Khwaldia, Enhanced functional properties of chitosan films cross-linked by biosourced dicarboxylic acids, Polym. Sci. Ser. A 58 (2016) 409–418.
[23] D.D. Ojeda-Hernández, U. Gomez-Pinedo, M.A. Hernández-Sapiéns, A.A. Canales-Aguirre, H. Espinosa-Andrews, J. Matias-Guiu, Y. González–García, J.C. Mateos-Díaz, Biocompatibility of ferulic/succinic acid-grafted chitosan hydrogels for implantation after brain injury: a preliminary study, Mater. Sci. Eng.: C 121 (2021) 111806.
[24] I.A. Sogias, V.V. Khutoryanskiy, A.C. Williams, Exploring the factors affecting the solubility of chitosan in water, Macromol. Chem. Phys. 211 (2010) 426–433.
[25] T. Songkroh, H. Xie, W. Yu, X. Liu, G. Sun, X. Xu, X. Ma, Injectable *in situ* forming chitosan-based hydrogels for curcumin delivery, Macromol. Res. 23 (2015) 53–59.
[26] K. Delmar, H. Bianco-Peled, The dramatic effect of small pH changes on the properties of chitosan hydrogels crosslinked with genipin, Carbohydr. Polym. 127 (2015) 28–37.
[27] E. Curotto, F. Aros, Quantitative determination of chitosan and the percentage of free amino groups, Anal. Biochem. 211 (1993) 240–241.
[28] U. Gómez-Pinedo, L. Sanchez-Rojas, M.S. Benito-Martin, C. Lendinez, G. León-Espinosa, F.J. Rascón-Ramirez, J. Herrero, B. Castro, L. Moreno-Jiménez, M. del Olmo, J.A. Matias-Guiu, J. Matias-Guiu, J.A. Barcia, Evaluation of the safety and efficacy of the therapeutic potential of adipose-derived stem cells injected in the cerebral ischemic penumbra, J. Stroke Cerebrovasc. Dis. 27 (2018) 2453–2465.
[29] K. Jeong, W. Lee, J. Cha, C.R. Park, Y.W. Cho, I.C. Kwon, Regioselective succinylation and gelation behavior of glycol chitosan, Macromol. Res. 16 (2008) 57–61.
[30] S. Woranuch, R. Yoksan, Preparation, characterization and antioxidant property of water-soluble ferulic acid grafted chitosan, Carbohydr. Polym. 96 (2013) 495–502.
[31] J. Zhu, H. Wu, Q. Sun, Preparation of crosslinked active bilayer film based on chitosan and alginate for regulating ascorbate-glutathione cycle of postharvest cherry tomato (Lycopersicon esculentum), Int. J. Biol. Macromol. 130 (2019) 584–594.
[32] M. Anwar, K. Nisa, N. Indirayati, Acid-base evaluation of chitosan-ferulic acid conjugate by a free radical grafting method, IOP Conf. Ser.: Earth Environ. Sci. (251) (2019) 012023.
[33] T. Pol, W. Chonkaew, L. Hocharoen, N. Niamnont, N. Butkhot, Y.M. Roshorm, S. Kiatkamjornwong, V.P. Hoven, K. Pratumyot, Amphiphilic chitosan bearing double palmitoyl chains and quaternary ammonium moieties as a nanocarrier for plasmid DNA, ACS Omega 7 (2022) 10056–10068.
[34] F.-L. Mi, S.-S. Shyu, C.-K. Peng, Characterization of ring-opening polymerization of genipin and pH-dependent cross-linking reactions between chitosan and genipin, J. Polym. Sci. Part A: Polym. Chem. 43 (2005) 1985–2000.
[35] I. Gonçalves, C. Nunes, S. Mendes, L.O. Martins, P. Ferreira, M.A. Coimbra, CotA laccase-ABTS/hydrogen peroxide system: an efficient approach to produce active and decolorized chitosan-genipin films, Carbohydr. Polym. 175 (2017) 628–635.
[36] F.-L. Mi, H.-W. Sung, S.-S. Shyu, Release of indomethacin from a novel chitosan microsphere prepared by a naturally occurring crosslinker: examination of crosslinking and polycation–anionic drug interaction, J. Appl. Polym. Sci. 81 (2001) 1700–1711.
[37] S. Teimouri, C. Dekiwadia, S. Kasapis, Decoupling diffusion and macromolecular relaxation in the release of vitamin B6 from genipin-crosslinked whey protein networks, Food Chem. 346 (2021) 128886.
[38] J. Andrade del Olmo, L. Pérez-Álvarez, V. Sáez-Martínez, S. Benito-Cid, L. Ruiz-Rubio, R. Pérez-González, J.L. Vilas-Vilela, J.M. Alonso, Wound healing and antibacterial chitosan-genipin hydrogels with controlled drug delivery for synergistic anti-inflammatory activity, Int. J. Biol. Macromol. 203 (2022) 679–694.
[39] M. Arteche Pujana, L. Pérez-Álvarez, L.C. Cesteros Iturbe, I. Katime, Biodegradable chitosan nanogels crosslinked with genipin, Carbohydr. Polym. 94 (2013) 836–842.
[40] F.-L. Mi, H.-W. Sung, S.-S. Shyu, Synthesis and characterization of a novel chitosan-based network prepared using naturally occurring crosslinker, J. Polym. Sci. Part A: Polym. Chem. 38 (2000) 2804–2814.
[41] E. Rossi, J.A.Á. Ramírez, M.I. Errea, Preparation of an environmentally friendly lead adsorbent. A contribution to the rational design of heavy metal adsorbents, J. Environ. Chem. Eng. 8 (2020) 104210.
[42] S.J. Lee, M.-S. Kang, J.-S. Oh, H.S. Na, Y.J. Lim, Y.-I. Jeong, H.C. Lee, Caffeic acid–conjugated chitosan derivatives and their anti-tumor activity, Arch. Pharm. Res. 36 (2013) 1437–1446.
[43] M. Xie, B. Hu, Y. Wang, X. Zeng, Grafting of gallic acid onto chitosan enhances antioxidant activities and alters rheological properties of the copolymer, J. Agric. Food Chem. 62 (2014) 9128–9136.
[44] M. Yan, B. Li, X. Zhao, J. Yi, Physicochemical properties of gelatin gels from walleye pollock (Theragra chalcogramma) skin cross-linked by gallic acid and rutin, Food Hydrocoll. 25 (2011) 907–914.
[45] J. Liu, C.-g. Meng, X.-c. Wang, Y. Chen, J. Kan, C.-h. Jin, Effect of protocatechuic acid-grafted-chitosan coating on the postharvest quality of Pleurotus eryngii, J. Agric. Food Chem. 64 (2016) 7225–7233.
[46] A. Sáenz-Galindo, L. López-López, I. F.de la Cruz-Duran, N. A.Castañeda-Facio, O. L.Rámirez-Mendoza, A. K.Córdova-Cisneros, C. D.d.Loera-Carrera, Applications of carboxylic acids in organic synthesis, in: B. Georgiana Ileana, R. Gabriel Lucian (Eds.), Nanotechnology and Polymers, Carboxylic Acid, IntechOpen, Rijeka, 2018 Ch. 3.
[47] C.W Guo Q, Y. Yang, Q.P. Li, Y.M. Ha, Preparation, structural characterization and functional properties of chitosan derivative, J. Food Technol. 3 (2018) 84–90.
[48] L. Danielyan, R. Schäfer, A. von Ameln-Mayerhofer, M. Buadze, J. Geisler, T. Klopfer, U. Burkhardt, B. Proksch, S. Verleysdonk, M. Ayturan, G.H. Buniatian, C.H. Gleiter, W.H. Frey, Intranasal delivery of cells to the brain, Eur. J. Cell Biol. 88 (2009) 315–324.
[49] C. Galeano, Z. Qiu, A. Mishra, S.L. Farnsworth, J.J. Hemmi, A. Moreira, P. Edenhoffer, P.J. Hornsby, The route by which intranasally delivered stem cells enter the central nervous system, Cell Transplant 27 (2018) 501–514.
[50] L. Salade, N. Wauthoz, J. Goole, K. Amighi, How to characterize a nasal product. The state of the art of *in vitro* and ex vivo specific methods, Int. J. Pharm. 561 (2019) 47–65.
[51] P. Dan, É. Velot, G. Francius, P. Menu, V. Decot, Human-derived extracellular matrix from Wharton's jelly: an untapped substrate to build up a standardized and homogeneous coating for vascular engineering, Acta Biomater. 48 (2017) 227–237.
[52] A. Basiri, M. Farokhi, M. Azami, S. Ebrahimi-Barough, A. Mohamadnia, M. Rashtbar, E. Hasanzadeh, N. Mahmoodi, M. Baghaban Eslaminejad, J. Ai, A silk fibroin/decellularized extract of Wharton's jelly hydrogel intended for cartilage tissue engineering, Prog. Biomater. 8 (2019) 31–42.
[53] H. Hao, G. Chen, J. Liu, D. Ti, Y. Zhao, S. Xu, X. Fu, W. Han, Culturing on Wharton's jelly extract delays mesenchymal stem cell senescence through p53 and p16INK4a/pRb pathways, PLoS ONE 8 (2013) e58314.
[54] E. Gao, Y. Wang, P. Wang, Q. Wang, Y. Wei, D. Song, H. Xu, J. Ding, Y. Xu, H. Xia, R. Chen, L. Duan, C-shaped cartilage development using Wharton's jelly-derived hydrogels to assemble a highly biomimetic neotrachea for use in circumferential tracheal reconstruction, Adv. Funct. Mater. 33 (2023) 2212830.
[55] E. Zand, E. Rajablou, S.F. Siadat, B. Beiki, V. Akbarinejad, C.A. Amorim, M. Rezazadeh Valojerdi, L.A. Tahaei, R. Fathi, Successful 3D culture and transplantation of mouse isolated preantral follicles in hydrogel of bioengineered Wharton's jelly, PLoS ONE 18 (2023) e0290095.
[56] K. Sobolewski, E. Bańkowski, L. Chyczewski, S. Jaworski, Collagen and glycosaminoglycans of Wharton's jelly, Biol. Neonate 71 (1997) 11–21.
[57] M. Nurunnabi, V. Revuri, K.M. Huh, Y.-k. Lee, Chapter 14 - Polysaccharide based nano/microformulation: an effective and versatile oral drug delivery system, in: E. Andronescu, A.M. Grumezescu (Eds.), Nanostructures for Oral Medicine, Elsevier, 2017, pp. 409–433.
[58] L.C. Wang, X.G. Chen, C.S. Liu, P.W. Li, Y.M. Zhou, Dissociation behaviors of carboxyl and amine groups on carboxymethyl-chitosan in aqueous system, J. Polym. Sci. Part B: Polym. Phys. 46 (2008) 1419–1429.
[59] L. Meng-Jen, T. May-Jywan, C. Wen-Chi, H. Wang-Yu, H. Chien-Hui, Y.-T. Chen, T. Tsung-Hsi, S. Chih-Hung, C. Ching-Jung, H. Cheng, Exogenous FGF-1 differently regulates oligodendrocyte replenishment in an SCI repair model and cultured cells, Biomedicines 10 (2022) 2724.
[60] Chen Y, Y. Liu, J. Xie, Q. Zheng, P. Yue, L. Chen, P. Hu, M Yang, Nose-to-brain delivery by nanosuspensions-based *in situ* gel for breviscapine, Int. J. Nanomed. 15 (2020) 10435–10451.
[61] F. Zahir-Jouzdani, J.D. Wolf, F. Atyabi, A. Bernkop-Schnürch, In situ gelling and mucoadhesive polymers: why do they need each other? Expert Opin. Drug Deliv. 15 (2018) 1007–1019.